Journal Pre-proof

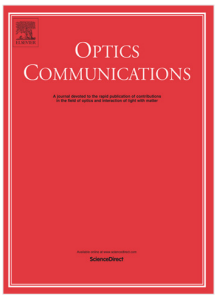

Unveiling Fourier Ptychography via Fisher Information

Juan M. Bujjamer, Hernán E. Grecco

PII: S0030-4018(20)31060-9
DOI: https://doi.org/10.1016/j.optcom.2020.126642
Reference: OPTICS 126642

To appear in: *Optics Communications*

Received date : 3 September 2020
Revised date : 10 November 2020
Accepted date : 22 November 2020

Please cite this article as: J.M. Bujjamer and H.E. Grecco, Unveiling Fourier Ptychography via Fisher Information, *Optics Communications* (2020), doi: https://doi.org/10.1016/j.optcom.2020.126642.

Unveiling Fourier Ptychography via Fisher Information

Juan M. Bujjamer, Hernán E. Grecco[‡]

November 5, 2020

Abstract

In recent years, Fourier Ptychographic Microscopy (FPM) has been demonstrated for a wide variety of applications including wide field of view pathology and quantitative phase imaging. Briefly, this technique produces a high resolution reconstruction by computationally combining a set of diversely acquired captures of the same sample. However, the nonlinear aspects of the algorithm and the noise in a typical dataset affect the reconstruction quality. The ability to weight differentially each image within an entire FPM capture would allow to device an optimal design of an acquisition platform and to potentially avoid such reconstruction problems.

Currently there is no method to calculate the information content of each capture and therefore to weight it accordingly. In this work, we propose such a method based on the concept of Fisher Information, not available until now for FPM acquisitions. This criterion depends on the selection of a sample model and the parameters to be measured in an FPM experiment. We show the application of our technique to two common problems: volume quantification using phase images and distance determination between two particles, both revealing interesting internal aspects of Ptychography. The approach used here could lead to an improvement of the speed in the acquisition and reconstruction process by making a more efficient selection of the illumination angles.

1 Introduction

Fourier Ptychographic Microscopy is a powerful technique recently developed [1] that allows to increase the resolution of an existent microscope without the addition of neither complex nor expensive optomechanical parts. While it shares some similarities with Structured Illumination Microscopy [2] as it restores the information in modulated versions of the pupil, FPM isn't limited to increasing the resolution of a microscope. It has also the invaluable advantage of recovering the phase of the complex sample, as the reconstruction approach is rooted in phase retrieval algorithms [3], originally adapted from their first applications to kinoforms and X-ray imaging to the optical microscopy oriented form. The starting point of a typical FPM acquisition is a set of low resolution but wide field of view images incorporating some kind of *phase diversity* [4] with the objective to increase the Space-Bandwidth product [2] of the original acquisitions. Building a wide field of view image with a high information content, FPM is an excellent tool in experiments where big data images are needed such as in digital pathology [5] as they provide full tissue images with subcellular resolution and both absorption and phase information of the samples.

Several methods have been used in order to provide phase diversity, such as tilted illumination [1], pupil defocusing [6], or coded masks [7]. In all cases, the reconstruction process requires a certain amount of overlap on the information of consecutive pupils, some minimum signal to noise ratio on the captured images and the knowledge of the illumination parameters (i.e. illumination angle for tilted angle FPM), else the uncertainties will propagate as reconstruction errors in the best case or fail to converge in the worst scenario. As convergence of phase retrieval algorithms are non-convex problems which are very sensitive to experimental conditions and the samples

*Juan M. Bujjamer and Hernán Grecco are with the Laboratorio de Electrónica Cuántica, at the Dpto. de Física, FCEN, Nuñez, Buenos Aires, Argentina (P.C. 1428) e-mail: (jubujjamer@df.uba.ar, hgrecco@df.uba.ar).
†

themselves, the error propagation for every possible case is mostly corrected [8] or optimized [9] heuristically. It is also difficult to establish *a priori* the amount of overlap needed for the images to converge [10] or how the image spectrum affects in the reconstruction.

Here we propose a method based on the concept of Fisher Information Matrix (FIM) to evaluate the information content of each image of an FPM acquisition. As a statistical parametric approach it is inherently independent on the reconstruction algorithms so that it is perfectly suited to evaluate the quality of the images prior to their processing. We base our work in the computation of the FIM applied to the estimation of parameters in a single molecule detection experiment [11], in order to do so we computed it in more complex shape forms and arbitrary illumination sources as FPM requires. In order to better visualize these matrices for multiple images, we arrange the FIM values in 2D image-like structures that condense them all, allowing a fast representation of the data contained in each full acquisition. We demonstrate the practical use of these arrays in the analysis of three selected experiments, and finally propose FIM as an experimental optimization tool to tailor the illuminator fitting it to the actual imaging needs.

In this work, we start in section 3 by reviewing the technique of tilted angle FPM and pointing some of the key aspects to obtain a good quality reconstruction. We then define the Fisher Information Matrix and calculate it numerically for the FPM acquisition process in section 4. The method is efficient to compute and just needs from the user to input its sample model, as the acquisition pupil computation is separated from the image model calculus. These results are applied in section 5 to quantify the weight of each captured image to the final reconstruction in some relevant applications such as cell volume quantification and particle distance measuring. Finally, an additional arbitrary image model is implemented, showing an alternative to the analytical modeling of the samples that can be useful in a more flexible approach.

2 Related Work

The idea application of Fisher Information to the FPM problem was inspired from the Single Molecule estimation case [11] which has a widespread application in superresolution techniques and subdiffraction imaging. It is also related to other related microscopy techniques such as lifetime measurement [12] and proposing a redefinition of the Raygleigh's criterion [13]. As far as we are concerned, there hasn't been calculated for the problem of Fourier Ptychography where its use is revealing in many aspects. There have been approaches to correct defects in the misalignments of the optical setups [14], to measure the minimal sampling criteria [15] and to correct pupil aberrations but all of them are based in minimizing the reconstruction error and therefore depend on the reconstruction algorithms. Additionally, there are techniques to use content-aware FPM acquisitions [16] [17] [18] by measuring the SNR of the acquired images or reporting a decrease in the acquisition and processing time.

We developed an objective-oriented approach that can be used in a variety of cases that allow to deepen the knowledge of the information content in FPM experiments. It answers practical estimation questions such as where the refractive index and width information is placed, whether a sampling could provide information on volume determination or distinguish phase from absorption.

3 Fourier Ptychography

The quality of an optical system is given by its maximum acceptance angle of diffracted light, which is quantified by the numerical aperture (NA) and the illumination wavelength λ. It can be thought of as a building block characterized by a transfer function (the Optical Transfer Function or OTF), which in the simplest case is a constant disc of radius $\mathrm{NA}/2\lambda$ in Fourier Space (a top-hat low-pass filter). The task is to increase the low-pass frequency of the OTF, but in order to do so the missing information at the dark positions has to be found.

Fortunately, there is one simple technique to sample all the missing spectrum of the image one disk at a time by sequentially shifting the OTF. It can be seen as the 2D version demodulating a radio signal a band at a time, and has the advantage that can be experimentally implemented with ease in a working microscope. In the proposed setup [1], the starting illumination wave direction is given by the wavevector $\boldsymbol{k}_0$ and is tilted in the direction of $\boldsymbol{k}_1$. The resulting wavefront will contain

this newly incorporated phase factor $e^{i\boldsymbol{k}_0\boldsymbol{x}}e^{i\boldsymbol{k}_1\boldsymbol{x}}$ which corresponds to a rigid shift of the OTF by properties of the Fourier Transform. In this way, the input angle of the wavefront translates to a shifting of the Transfer Function, and this allows to sample the spectrum in circular windows by just changing the illumination angle. The most common optical setup for tilted FPM consists of a LED Matrix as shown in Figure 1, where the complete acquisition/reconstruction process is schemed. The idea is to capture images one LED at a time, where each LED_{ij} is defined by a wavevector $\boldsymbol{k}_{ij}$. The $n \times n$ LEDs in the matrix array give the same amount of poorly resolved images covering the area of a new synthetic numerical aperture. This data is finally entered to an iterative phase retrieval algorithm whose output is the complex reconstructed image.

Generally speaking, this is a way to incorporate what is called *phase diversity*, which means that the sampling probe has to contain some degree of wavefront distortion [4]. In this case, we provided phase diversity to the samples by varying the angle of a planar wavefront, and we shall mention it in the following as *tilted* FPM. It is necessary to mention at this point that the shifting property of the spectrum is based on a thin object approximation, where the effect of the incoming lightwave can be approximated to a product with the sample. This approximation holds for typical biological samples but could also be made exactly true with techniques like aperture-scanning FPM [19].

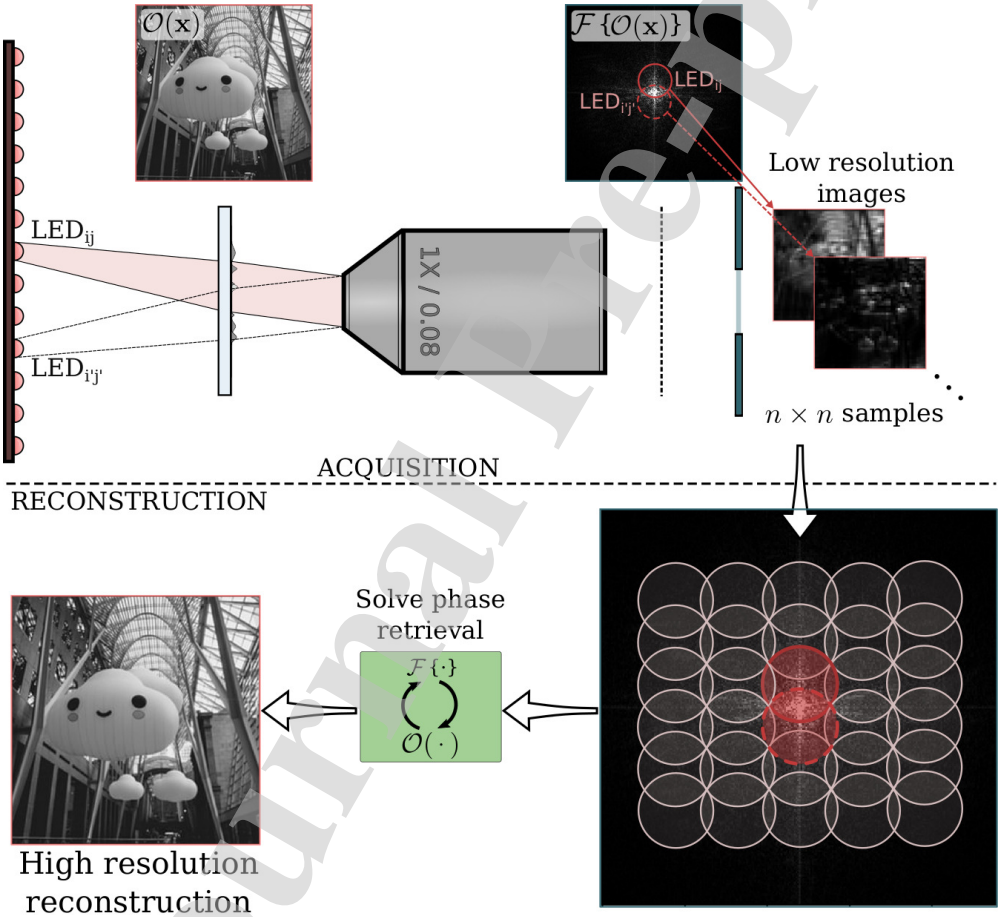

Figure 1: Complete tilted Fourier Ptychographic Microscopy setup showing acquisition and latter reconstruction. Using a LED matrix, an object $\mathcal{O}(\boldsymbol{x})$ is sampled at different angles, shifting the microscope pupil across the transformed space $\mathcal{F}\{\mathcal{O}(\boldsymbol{x})\}$. Then, the $n \times n$ low resolution images are stitched in place by means of the phase retrieval algorithm to recover the magnitude and phase of the higher resolved image.

As stated before, the building up of an image from this sampled sections of its magnitude-only

spectrum is enclosed in a wider set of solutions called *Phase Retrieval*. It involves finding the lost phase of the spectrum that carries the structural part of the spectrum (i.e. the relative position of each fragment in the original image). The task is then to reconstruct the phase of a sample from magnitude-only acquisitions, and in turn to increase the numerical aperture of the images at the maximum provided by these samples.

There is a great variety of reconstruction algorithms to solve the phase retrieval problem [20], among which those based on alternated projections stand out [21], such as the error-reduction [22] which we use in our reconstructions. The whole acquisition and reconstruction process is summarized in Figure 1. It starts with a random or empty guess of the complex output image and feed the initial state of the iterations. These imply the sequential replacement of the real space magnitude of the current solution by the corresponding measured samples, masking it with the known shifted pupil in Fourier space while keeping always the phase of the solution unaltered. After these steps are completed for the whole set of acquired images, the process is repeated again a number of times until convergence. The result is a better resolved magnitude image and the estimation of the phase information which freely converges to its true value to match the whole set of projections.

The tilted FPM setup is not difficult to build, but some considerations have to be taken in order to construct such systems. In the first place, in order for the phase retrieval algorithms to converge to a solution, there is a requirement of overlap among the shifted OTFs, i.e. there has to be a degree of *redundancy* on the data provided by neighboring pupils [15]. In the experimental setup, the overlap is given by the gap between the LEDs and the elevation of the sample holder with respect to the illuminator. On the other hand, constructive differences among different vendors and small misalignments in the light path usually result in imperfections of the reconstructed images ranging from a mild addition of noise to an direct impossibility of the algorithms to converge. The reason why the experimental imperfections impact on the quality of the final image in an unpredictable way is related to the nonlinear and non-convex characteristics of the problem. The iterative solutions, in turn, make the errors difficult to track and correct. In the next section we define the Fisher Information Matrix and calculate it for a phase diversity process as the one just stated.

4 Fisher Information of FPM

The Fisher Information Matrix (FIM) is a container of the knowledge about a set of estimated parameters and their correlation available in a data sample. It has been widely used in microscopy to evaluate the fundamental bounds in the estimation of the position of a single molecule, its intensity parameter and the minimum measurable distance between two particles [23]. The requirements that allow its calculation is the knowledge of the microscope OTF, and a model of the measurable image as a function of the estimated parameters.

The connection between the FIM and the minimum measurable values of the parameters relates to the Cramer-Rao Lower Bound (CRLB), which gives a lower constraint for the diagonal values in the covariance matrix of the estimator $\hat{\boldsymbol{\theta}}$ [24]

$$\mathrm{Cov}(\hat{\boldsymbol{\theta}}) \geq \mathcal{I}_{\boldsymbol{\theta}}^{-1}, \tag{1}$$

where $\boldsymbol{\theta}$ is the vector of parameters $(\theta_1, \ldots, \theta_p)$ to be estimated from the samples. The power of FIM relies on the fact of being independent of the estimator, it only reports which is the minimum variance that a particular set of parameters and data could possibly bring. In the context of FPM, this is extremely useful because it separates the reconstruction information from the reconstruction process itself.

4.1 Derivation of FIM for Fourier Ptychography

Each acquired image has a spectral-specific content related to its space distribution, and we can use the Fisher Information to characterize each of them. As illumination angles depart from central illumination, the intensity of the captured images become noisier and less intense, so the question is

to what extent these images are important for the reconstruction process and what is the structure of the FIM as a function of the pupil position in Fourier space.

The derivation of the Fisher Information Matrix of the set of parameters θ with an arbitrary noise process characterized by a mean of photons arrival of $E[N(t)]$ and an efficiency factor of γ for the detection process is given by [23]

$$\mathcal{I}_\theta = \gamma E[N(t)] \int_{\mathcal{R}^2} \frac{1}{q(\boldsymbol{\theta}, \boldsymbol{x})} \left(\frac{\partial q(\boldsymbol{\theta}, \boldsymbol{x})}{\partial \boldsymbol{\theta}} \right)^T \left(\frac{\partial q(\boldsymbol{\theta}, \boldsymbol{x})}{\partial \boldsymbol{\theta}} \right) d\boldsymbol{x}, \tag{2}$$

where $q(\boldsymbol{\theta}, \boldsymbol{x})$ is the *image distribution function* which can be calculated from both the structure of the sample and the illumination in the acquisition process and as a distribution it has to be normalized. From this expression it is clear the temporal contribution of the noise and the spatial distribution due to the sample shape and the optical transfer function can be calculated independently. We note that the use of this expression has a slightly different interpretation than that of the single molecule bibliography: in our case we illuminate the sample with a point source that provides a constant light intensity over the sample, and that is what defines the temporal statistics of the illuminator. Then we treat the sample, the shifting pupil and the microscope as a transfer function contained in the Image Distribution Function, which we vary in order to simulate different experiments. This can be done as long as these functions satisfy the regularity conditions needed to calculate the Fisher Information integral [25] and there is no interdependence among the image function parameters and those of the temporal distribution.

4.2 The Image Distribution Function

Let us consider an experiment where there is an object with a complex transmission function given by $\mathcal{O}(\boldsymbol{\theta}, \boldsymbol{x})$, where the parameters $\boldsymbol{\theta}$ are considered unknowns of the problem we wish to estimate. For example, in the case where the object is composed of a pair of cells modeled as two Gaussian functions, the set of parameters could be the location of both particles and the distance among them $\boldsymbol{\theta} = (x_0, y_0, x_1, y_1, d)$. It is a fact that in this case both positions are correlated to the distance among them, but that does not mean there is a contradiction in the problem specification, it is certainly expected that the correlation would be an output of the calculation.

The image distribution function can be calculated from the object itself and the Point Spread Function (PSF) of the system, noted as $t(\boldsymbol{x})$. To get each Fourier Ptychographic image, a convolution occurs between the object and the PSF

$$s(\boldsymbol{\theta}, \boldsymbol{x}) = \mathcal{O}(\boldsymbol{\theta}, \boldsymbol{x}) \circledast t_p(\boldsymbol{x}), \tag{3}$$

where the p subindex of the PSF that accounts for rigid shifting in Fourier Space. Note that $\mathcal{O}(\boldsymbol{\theta}, \boldsymbol{x})$ is explicitly dependent on the parameters, but $t_p(\boldsymbol{x})$ is not, as the optical system is independent on the parameters of the image(on the position of a molecule, for example).

In the most simple case, with no aberrations of any kind, the pupil is a circular aperture of radius given by $k_0 = 2\pi NA/\lambda$. The shift of the pupil corresponds to an addition of a phase $\boldsymbol{k}_s$, so for an arbitrary FPM image one can write

$$s(\boldsymbol{\theta}, \boldsymbol{x}) = A_0 \mathcal{O}(\boldsymbol{\theta}, \boldsymbol{x}) \circledast \frac{J_1(\boldsymbol{k}_0 \boldsymbol{r})}{r} e^{i\boldsymbol{k}_s \boldsymbol{r}}, \tag{4}$$

here A_0 is an integral normalizing factor and $J_1(\cdot)$ is the Bessel function of the first kind which comes from the Fourier Transform of the circular aperture.

The expression of FIM for a Poisson process in equation (2) requires taking partial derivatives with respect to each considered parameter. As in our convolution model the PSF functions $t_p(\boldsymbol{x})$ are independent of the parameters, the only partial derivatives to calculate is the one of the object with respect to each parameter θ_i

$$\frac{\partial s(\theta_i, \boldsymbol{x})}{\partial \theta_i} = \frac{\partial \mathcal{O}(\theta_i, \boldsymbol{x})}{\partial \theta_i} \circledast t_p(\boldsymbol{x}), \tag{5}$$

which simplifies FIM calculation for a general FPM case. As the image distribution function is the detected photon signal, it is proportional to the intensity of the input waveform so can be obtained

as $q(\boldsymbol{\theta}, \boldsymbol{x}) = s(\boldsymbol{\theta}, \boldsymbol{x})s^*(\boldsymbol{\theta}, \boldsymbol{x})$, it is a 2D spatial distribution function and should be normalized [26]. Finally, the derivative of the image distribution function of (2) can be obtained by just applying the product rule

$$\frac{\partial q(\boldsymbol{\theta}, \boldsymbol{x})}{\partial \theta_i} = \frac{\partial s(\boldsymbol{\theta}, \boldsymbol{x})}{\partial \theta_i} s^*(\boldsymbol{\theta}, \boldsymbol{x}) + s(\boldsymbol{\theta}, \boldsymbol{x}) \frac{\partial s^*(\boldsymbol{\theta}, \boldsymbol{x})}{\partial \theta_i} \tag{6}$$

The case where $s(\boldsymbol{\theta}, \boldsymbol{x})$ is a delta function [11] is derived here as a limiting case of a Gaussian distribution of infinitesimal width. Thus, calculating the FIM for the FPM acquisition process is only slightly more involved than doing so for the single particle bright field case due to the convolution properties on the derivatives. Moreover, as derivatives are taken only in the image function it is not necessary to calculate the derivatives of the Airy function so the equation 4 can be calculated faster using the inverse Fourier transform with a circular pupil.

4.3 Temporal distribution Function

In (2) there is the prefactor $\gamma E[N(t)]$ related to the temporal distribution of noise and while is treated in [11] in detail we include it here to complete the picture. Without incorporating detector noise of any kind, photons arriving to any pixel of a photodetector can be modeled as a Poisson process with expected value $\Lambda(t)$ because of their pure stochastic quantum nature. In many experiments, the so called intensity distribution λ can be considered constant for the process and so $\Lambda(t) = \lambda \Delta t$. In a more general framework, its time variant counterpart can account for effects like photobleaching, intensity oscillation of biomarkers or other dynamical processes [27]. In practice, detectors are discretized and spatially distributed over a detection area, and each one associated with an intensity parameter λ_k. As seen in section 4.2, the distribution of intensities over the pixels of the sensor can be determined by the Image Distribution Function $q(\boldsymbol{\theta}, \boldsymbol{x})$.

Considering a real photodetector, there are some incremental sources of noise worth considering. In the first place, the existence of dark currents of thermally generated electrons which are virtually indistinguishable from their photon generated counterparts. These are also modeled by a Poisson process with constant intensity parameter μ_k, where the k index refers to each of the pixels in the detector. The same process can absorb other sources of Poisson noise independent of the one given by the photon arrival, such as autofluorescence. As the sum of independent Poisson random variables result in another Poisson random variable, it is convenient to absorb all the previously mentioned sources of noise into one with parameter $\nu_k = \lambda_k + \mu_k$.

Detection electronics usually add some of its own noise to the final acquisition. It can come from many sources, such as Johnson noise or reference voltage fluctuations [28]. These additional noise processes are modelled with a Gaussian distribution $N_e \propto \mathcal{N}(\eta_e, \sigma_e)$ where η_e and σ_e are the mean and deviation respectively. Here it is assumed that the Gaussian distribution has the same parameters over the complete set of pixels, in spite of the fact that particularly in the case of CMOS detectors amplification electronics is not shared and could potentially have different noise distributions for each of the k pixels.

The combined form of the contributions is the addition of Poisson and Gaussian random variables, so the resulting probability distribution function can be calculated as the convolution of them [11]

$$p_Z(z) = \frac{e^{-\nu_k}}{\sqrt{2\pi}\sigma_e} \sum_{l=0}^{\infty} \frac{\nu_k^l}{l!} e^{-\frac{-(x-l-\eta_e)^2}{2\sigma_e^2}} \tag{7}$$

We are interested in the estimation of the image distribution parameters, so in order to calculate the FIM we only need the expected value of the counting process which can be calculated from the distribution in equation (7). In the following sections this value will remain constant as illumination parameters are not considered to change during the experiment. The relative width and the mean values of noise for these different cases is shown in Figure (2) in the image simulation of a single molecule. Note that more elevated photon counts return also more noise variance because of the Poisson nature of the process and also becomes more Gaussian-like.

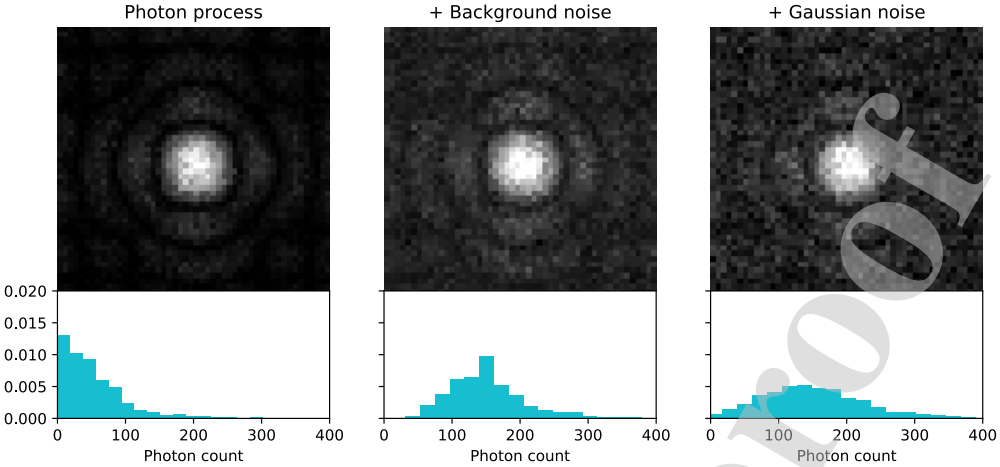

Figure 2: Simulated PSF images with incremental levels of noise, showing the incremental variance and distribution in a real imaging environment. The image on the left accounts just for Photon distribution, the middle incorporates background Poisson noise and finally Gaussian noise added at the rightmost image.

5 Applying Fisher Information to a complete FPM acquisition

Once the spatial and temporal terms of the FIM were calculated, the complete matrix for a single image can be obtained using (2). As one single FPM acquisition consists of a set of $N = n \times x$ independent images, the complete information of an acquisition can be calculated from the sum of the individual matrices. In the estimation of p parameters, we use the notation

$$\mathcal{I}_\theta^{ij} = \begin{pmatrix} \mathcal{I}_{11} & \cdots & \mathcal{I}_{1p} \\ & \ddots & \\ \mathcal{I}_{p1} & \cdots & \mathcal{I}_{pp}, \end{pmatrix} \tag{8}$$

to indicate the FIM of a single measured image, adding a superscript indicating the index of the illumination array. We deliberately omit the indexes when referring to the matrix elements in order to simplify the notation.

As we want to emphasize the variation of the elements with the illumination angle, we arranged their values in matrices as shown in Figure 3. This ordering of the FIM values as an image shows the relative weight of each tilted image to the total information. A total of $p(p/2-1)$ matrices $\mathcal{I}_{ij}$ can be constructed using the same strategy as the FIM is symmetric. Nevertheless, in most applications, the only contributing valuable information are the diagonals, as we will see later.

Not only the total information, but the structure of these matrices have an important meaning, as each of its elements are related to the relevance of an image to the particular estimation process. Taking it as an example, in Figure 3 a green pixel in position $i'j'$ represents the information value for the $\text{LED}_{i'j'}$ which is lower than the value for LED_{ij}. In the particular example of Figure 3, the center illuminators appear to have the most informative values for the parameter considered, a fact that in FPM is not always true as we shall see later. By looking at the resulting matrix, it is clear that the discretization of information in the image is given by the LED array and this directly impacts in how accurate the image model has to be in order to correctly represent the actual experiment.

As for the statistical meaning of these parameters, notice that the reciprocal of the FIM matrix is the CRLB (1), which yields the best achievable deviation of each parameter in the model. The p corresponding matrices for the diagonals of the $Cov(\hat{\boldsymbol{\theta}})$ matrix could as well be represented using the same approach stated here. In the next sections we will look into a selection of examples showing how differently distributed the information can be in an FPM acquisition and how this

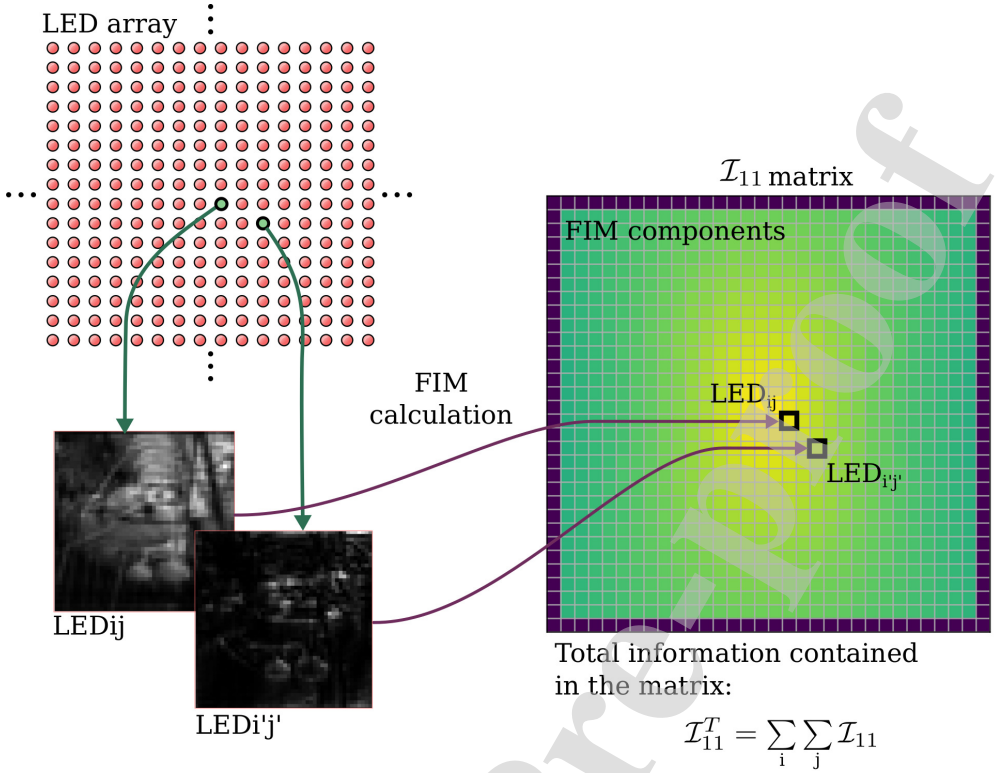

Figure 3: Construction of the FIM, showing how its structure parallels that of the LED matrix. An arbitrary image is acquired by turning on the LED$_{ij}$, then its complete FIM matrix is computed and each component is represented as a colormap image. The complete information matrix can be calculated by adding all its values.

depends on the estimated parameter.

5.1 Single molecule estimation in FPM

We first investigate the estimation of the position of a single molecule. This is a widespread application which can be applied to every microscopy setup, considering the tracked image is much smaller than the microscope PSF. It is also a good comparison case as it has been successfully solved for the transmission case [23] with a simple closed form. It can be seen [11] that the diagonals of the FIM for a single point emitting with an intensity parameter A is

$$\mathcal{I}_{11} = \mathcal{I}_{22} = \gamma A t k_0^2, \tag{9}$$

where an optical system with efficiency γ and an integration over a time t, and cut spatial frequency given by $k_0 = 2\pi NA/\lambda$ where considered. The fact that the matrix is diagonal is a result of the symmetry of the problem.

The same analysis can be performed over an FPM acquisition and despite the more complex illumination setup the result is also simple. Taking the estimated parameter to be the position of the particle $\theta = (x_0, y_0)$, being $\mathcal{O}(x, y) = \delta(x, y)$, the image distribution $q(x, y)$ does not change with the illumination angle, as the phase of the illumination source vanishes when taking modulus of $s(\boldsymbol{\theta}, x)$. To calculate the FIM for the complete acquisition, we use the property stating that information matrices of independent processes is the sum of the individual FIMs. So in the case of FPM using an array of $N = n \times n$ LEDs the resulting information for the complete acquisition is simply $\mathcal{I}_N = N\gamma A t k_0^2$, i.e. increases linearly with the number of images acquired. Note that one of

the characteristics of an FPM reconstruction with N images is an augmented synthetic numerical aperture NA_{syn}, so $\mathcal{I}_N$ can be compared to the information of a hypothetical system with a numerical aperture of NA_{syn}. From this we find that the number of images needed to achieve the same information quantity for the second case which can be calculated from the enhancement factor m as

$$N_{req} = \left\lceil \frac{NA_{syn}^2}{NA^2} \right\rceil = m^2. \tag{10}$$

The information contained in a microscopy image grows proportional to the square of its NA but linearly with the number of images, so it seems the convenience of using a better resolving objective rapidly surpasses that of taking more images. To provide an exemplifying case, we use a benchmark FPM setup consisting of a matrix with $N = 32 \times 32$ LEDs at a height of 80 mm from the sample and a separation LEDs of 6 mm combined with a microscope of $NA = .08$. It is not a case of strong redundancy, as this setup defines an OTF overlap of about 40% which means the pupils are close to the limit of their maximum separation. With such a system, a $NA_{syn} \approx .8$ can be reconstructed, and using equation (10) this leads to $N_{req} = 100$. The conclusion appears to be that for this task, the FPM technique seems to bring little information as it has about 10% the efficiency of an equivalent microscope of higher NA. As we will see later, this conclusion makes no justice to the complete capacities of FPM as localization is not the same as resolution.

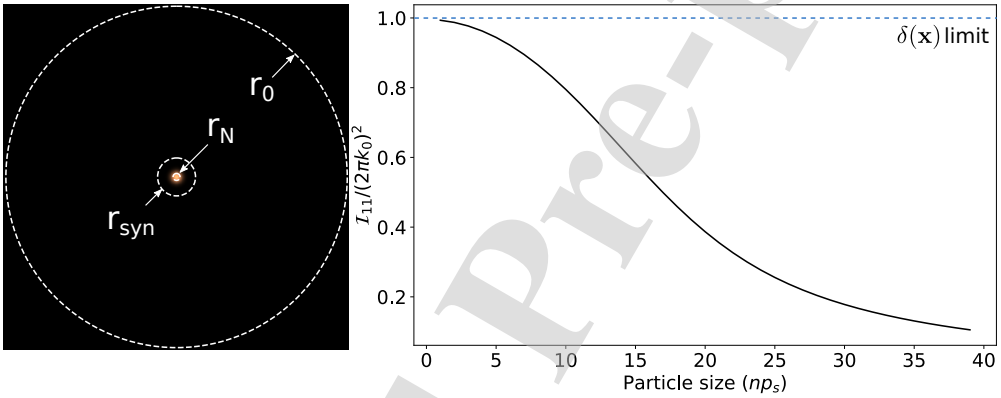

Figure 4: The estimation accuracy for the single particle case. At the left, the relative size of the position estimation variance for three optical setups: low NA (r_o), high synthetic NA (r_{syn}) and the complete set of N equally distributed independent images case (r_N). At the right it is shown the gradual lost of information while increasing the particle size (in pixel size multiples).

Using the approach of section 4.1 it is possible to calculate the FIM when the image function is no longer a delta. In this case not only information contained in an image tends to decrease, but also the symmetry conditions that diagonalize the Fisher Information Matrix no longer apply, even in cases where the object itself is symmetric (as a cause of the non-symmetric PSF). The gradual loss of information is shown in Figure 4 in the central transmission image, $\mathcal{I}_{11}$ is compared to k_0^2 because this is the limiting value for the delta case. The increase in particle size σ was performed in multiples of the pixel size. The reduction in the information content is related to the poorer localization of a wider Gaussian. At some point, the tails of the Gaussian start to fall off the image and so the estimation ability tend to zero for bigger widths.

When departing from the symmetric PSF, off-diagonal terms of the FIM start to appear. In Figure 5 the $\mathcal{I}_{ij}$ matrices are shown for this particular case. If no further indication is given, at the right and top of the matrices the central profiles in each direction are shown. The resulting matrices share some regularities that are good to emphasize. In the first place, the location of each coordinate is a rotated version of each other and as a result both diagonal terms are the rotated surfaces. On the other hand, FIM are always symmetrical so only one of the off-diagonals matrices is shown. The remaining element, highlighted with dotted lines, is the squared sum of the estimated variances calculated using the CRLB of equation (1). The inversion of the FIM also

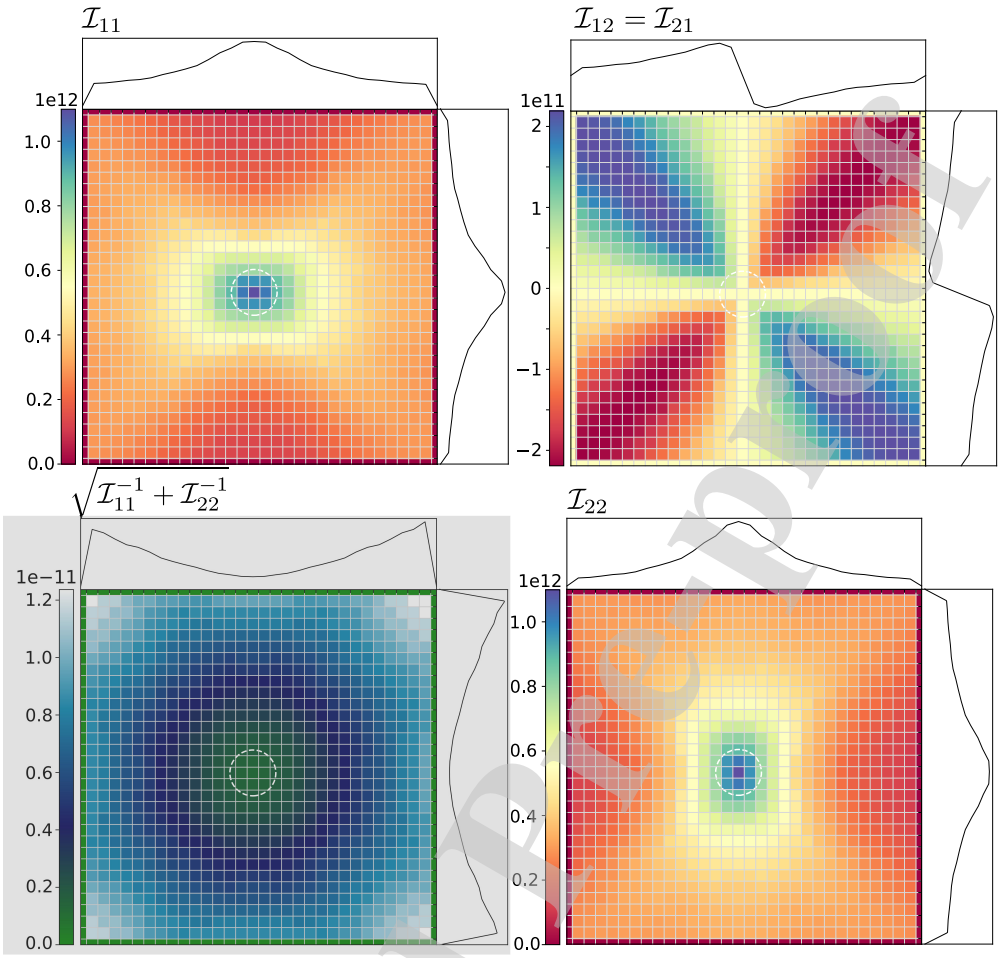

Figure 5: FIM matrices for the estimation of the position of a Gaussian shaped particle with a $5p_s$ width. As it departs from a delta function, the FIM matrix has now correlation among the x and y parameters and the information level start to decrease with the angle. In all cases the dashed circle shows the NA limit of the microscope and the center horizontal and vertical profiles of the images are ploted top and right of the figures respectively.

contains the information of the crossed terms and reports the least error in the determination of the total position determination for each of the FPM images. The magnitude of the off-diagonal elements is at least an order smaller than its diagonal counterparts so the effect of the correlations is small for this case. Nonetheless, it is important to note that every off-diagonal element is related to a correlation among the parameters of $\boldsymbol{\theta}$ and always lead to a degradation in the estimation of the diagonals of the covariance matrix.

5.2 Distance of two particles

A magnitude closely related to the resolution of an optical system is the estimation of the distance separating two particles. It is well known that the most popular definitions of optical resolution are based on this magnitude, so it is a suitable benchmark test to evaluate the structure of the FIM image for FPM. We start modelling two Gaussian particles of the same width σ

$$s_1(d, x, y) = \frac{1}{\pi\sigma^2} e^{-\frac{1}{2\sigma^2}} \cosh x^2 d/\sigma^2, \tag{11}$$

where d is the scalar separation in the direction of x and the only parameter to estimate from this model. Using the partial derivative against d we calculate the corresponding FIM and we show in Figure 6 that the increment of the numerical aperture of the system increases the information content of an image up to a plateau. This is consistent with the typical definition of resolution which is proportional to the NA of the optical system. The saturation zone starts at the point where the Gaussian is no longer limited by the PSF, or in other words, σ is greater than the radius of the Airy function.

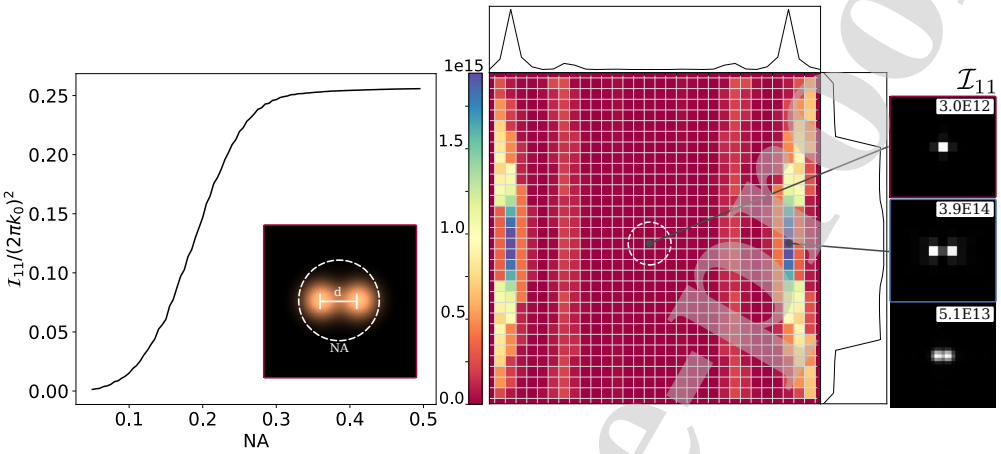

Figure 6: (left) Information content against numerical aperture of a transmission microscope, showing a high increase in the lower resolving zone and a plateau once the two particles can be resolved ($NA \approx 0.3$). (right) FIM image of the distance parameter with example images on two zones. The upper right image is the central acquisition where the information content is almost null and the two particles are totaly merged into one central spot. Contrarily, the image at the center lies in the zone of high information content where two particles are clearly distinguishable. The bottom image corresponds to the FPM reconstruction. In the three cases the number at the top indicates the information content of each image.

We simulated two particles separated with parameters $\sigma = 2.5p_s$ and $d = 2p_s$. Contrary to the case where a $\mathcal{O}(\theta) = \delta(\theta)$, the information content on the distance estimator is highly dependent on the illumination angle. In this example, the technique shows one of its remarkable properties of collecting information outside the numerical aperture of the microscope. It is clear that the portion inside the numerical aperture contains little information about distance as the particles are very poorly resolved for this NA value as seen in the right panel of Figure 6. On the contrary, there are some FPM images with high information quality particularly distributed near the NA circle. This is consistent with high speed FPM implementations that argue that the maximum information is often contained near the borders of the pupil [29].

It is also illustrative to compare the information content of each of the involved images. The central low resolution spot yields an information factor near 3×10^{12}, while the high resolution reconstruction raises it to 5.1×10^{13}, near a ten-fold improvement factor. Nevertheless, considering the complete set of low resolution images, the one containing the maximum information for the distance estimation is 3.9×10^{14} which is much higher than that of the high resolution image. This shows that depending on the application there is much room for improvement in the estimation using the same available information. In fact, the complete set of 960 images returns a total information of 4.9×10^{17}.

5.3 Measuring the phase of an object

One of the distinguishing properties of FPM is its ability to uncover the phase information from a magnitude observation. This is implicit in the model elaborated in section 4.1 and we consider it here to evaluate the information content of the FPM set. Phase quantification allows to measure volumes and refractive indices, and it is an useful application of FPM [30] specially in unstained

cell cultures. We can quantify the amount of information on volume contained in a complete FPM acquisition using a simple model of a Gaussian-shaped cell.

We model the phase of a single unstained cell with volume $v = 2\pi\sigma^2$ as

$$c(r) = A_0 e^{i\phi(\boldsymbol{r})}, \tag{12}$$

where the magnitude of the sample is a constant A_0 and its phase is a Gaussian function $\phi(\boldsymbol{r}) = e^{-\pi/vr}$. In a typical transmission microscope the image of the cell will be virtually transparent, as long as there is no absorption or scatter. In the real case, mild signals could be seen due to scattering, but we restrict our model to the non absorptive case. Some phase contrast techniques can be implemented in order to observe such samples but not all of them are quantitative and wouldn't allow to measure the volume of a particle. FPM is a technique that allows such measurements, along with other phase retrieval based methods, such as Differential Phase Contrast [30]. We calculated the FIM for the parameter v, assuming the position of the particle is known, as in the latter case. We construct the FIM image to assess the illumination angles carrying the most informative images. It can be clearly seen that the center of the FIM carries no information of the volume as there is null information on phase for the central LED. There is a region of little information inside the numerical aperture of the microscope, but jumping out of this central region $\mathcal{I}_v$ reaches its maximum value. This is consistent with newer implementations of fast FPM

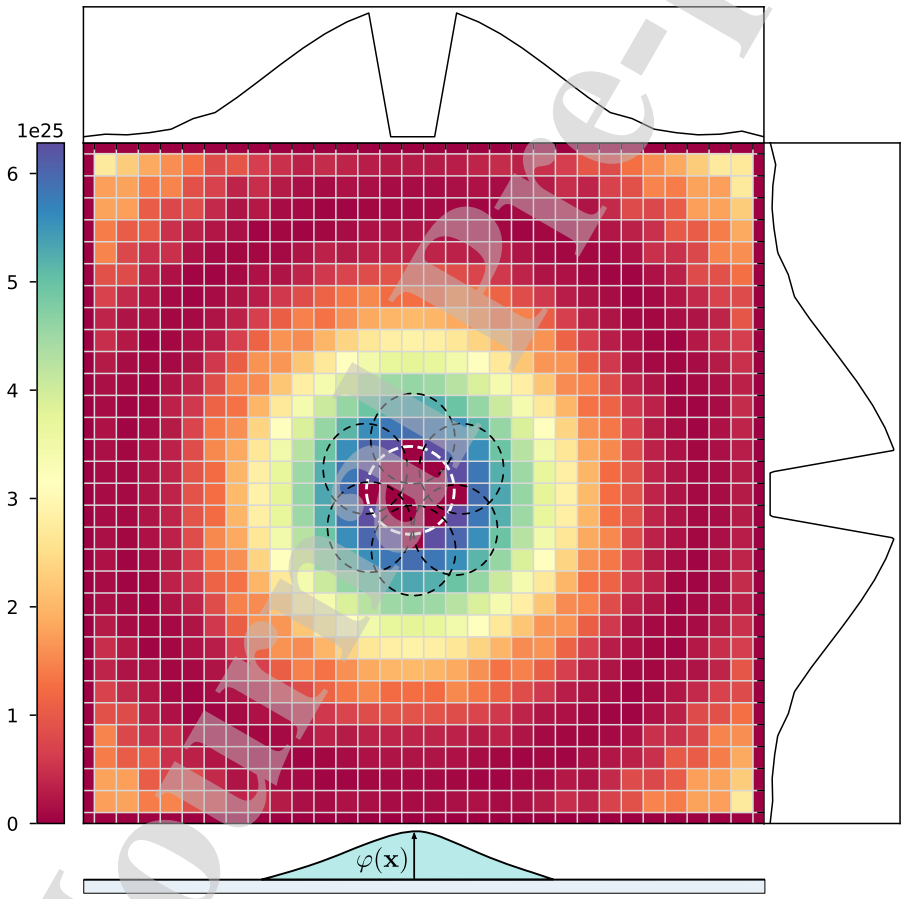

Figure 7: FIM of the volume estimation problem. The sample, schemed at the bottom is a Gaussian phase-only object. The information quantity is minimal inside the circle given by the NA (dashed white circle). The black dashed circles indicate six annular acquisitions, which is another FPM illumination technique, to compare it to the total information quantity.

acquisition that argue that the sample can be totally reconstructed by sampling just at the frontier of the NA [29] in annular illumination systems, in the case presented here an annular acquisition with just 6 images as shown in Figure 7 contains as much as the 40% of the total information on volume. In fact, sampling at the limits of the NA not only provides the highest information about the phase of the sample but also on the magnitude as such sampling technique also incorporates the central information.

Circular symmetry is related to the Gaussian model used to simulate the cell, and so is the linear decay from the borders to the limiting LEDs. This is by no means a restriction of the technique as any shape could be used in the simulation. As an example of this, in the next section we calculate the information contained in an arbitrary image using numerical differentiation.

6 Application to arbitrary images

We showed how the FIM evaluation of a sample can provide a quantitative determination of the most relevant illumination angles for a modeled image. It is a very useful tool in the preparation of an experiment with the correct model of the measured magnitude and phase, but it is true that the choice of the model and its calculation can be time consuming. Here we give an alternative approach to calculate the FIM of arbitrary samples based in a numerical computation of the partial derivatives in (5). This approach has the advantage that it is based on the morphology of the sample and so it needs only a sketch of its approximate shape. It also has the limitation that the only parameters considered are also morphological and so more restricted than the original functional version.

Let us consider an arbitrary object $g(\boldsymbol{x} - \boldsymbol{x}_0)$. To calculate numerically the partial derivatives with respect to $\theta = \boldsymbol{x}_0$ the computation of the gradient of the input image is performed, obtaining a value proportional to $\partial g(\boldsymbol{\theta}, \boldsymbol{x})/\partial \boldsymbol{x_0}$. As a result, the FIM of an arbitrary sample could be calculated as shown in Figure 8 and it is proportional to the information on the determination of the position of the shape considered. The information acquired from the FIM can be used in the incorporation of weights to each led in the FPM setup to emphasize the information corresponding to a desired shape. This could be used to sparsely sample the acquisition using only the most informative LEDs thus speeding up the acquisition and reconstruction time. Note that, as discussed in section 5 FIM is heavily discretized, so providing a sketch of the most prominent features of the measured sample is sufficient to find the most informative acquisitions to reconstruct the samples.

7 Conclusion

In this work, we proposed a method to measure the information quantity in a FPM experiment, methods as such are not available until now. As it is a parametric method, the key is to choose the right model to the specific estimation task, but the results are robust and easy to interpret. Here we showed its application to some simple models with few parameters, but the same method can be applied to any image function with any desired number of parameters being estimated at the same time. It remains to be shown how the addition of new parameters impact on the others, an effect that can be easily calculated from the off-diagonal elements of each FIM matrix.

In this case we decided to concentrate on FPM as the key application, but only changing the sampling PSF the same analysis can be applied to other methods. Of particular interest could be the case of DPC, where there can be some missing information near the axis of the asymmetrical pupil. By quantifying the missing information region, a more compact set of complementary pupils can be applied in order to minimize the errors [31]. We also expect that this concept could be extended to the 3D domain for cases where the thin sample approximation does not hold, as it is done in techniques like Fourier Ptychographic Diffraction Tomography (FPDT) [32].

We discussed and reviewed some theoretical aspects of FPM. On the one hand, we showed that augmenting the numerical aperture of a system is by no means equivalent to measuring with more resolution the position of one particle. The last application requires an extra knowledge of the system involved along with some sort of fitting, while the former is totally model independent and allows the system to better resolve unknown objects in the image space. FIM gives a visual demonstration that localization of a set of particles is not equivalent to augment the resolution

of a system, and that the need of previously modeling the positions of a set of known particles is a strong assumption that severely bound the problem. This is the reason why the single particle estimation appear to be so inefficient in the FPM case, as it takes extra images to recover lost phase information related to the position of unknown objects with arbitrary shapes. On the contrary, bright field measurement applied to the distance among two particles and on the volume estimation of a cell was shown to be much less informative than FPM even for the simple case of two particles. It is expected that loosing restrictions and allowing more independent variables in the problem show more contrasting behaviors.

As it needs an approximate model of the experiment, this technique could allow to optimize the acquisition and reconstruction time of ptychographic imaging by selecting the most informative acquisitions. These approximate models can be suited to a set of similar experiments, so it would be sufficient to precalculate one FIM image for a set of captures. In practical terms phase retrieval algorithms require that the overlap condition is fulfilled for a robust convergence of the images, so a special care has to be taken in order to use FIM as a masking approach.

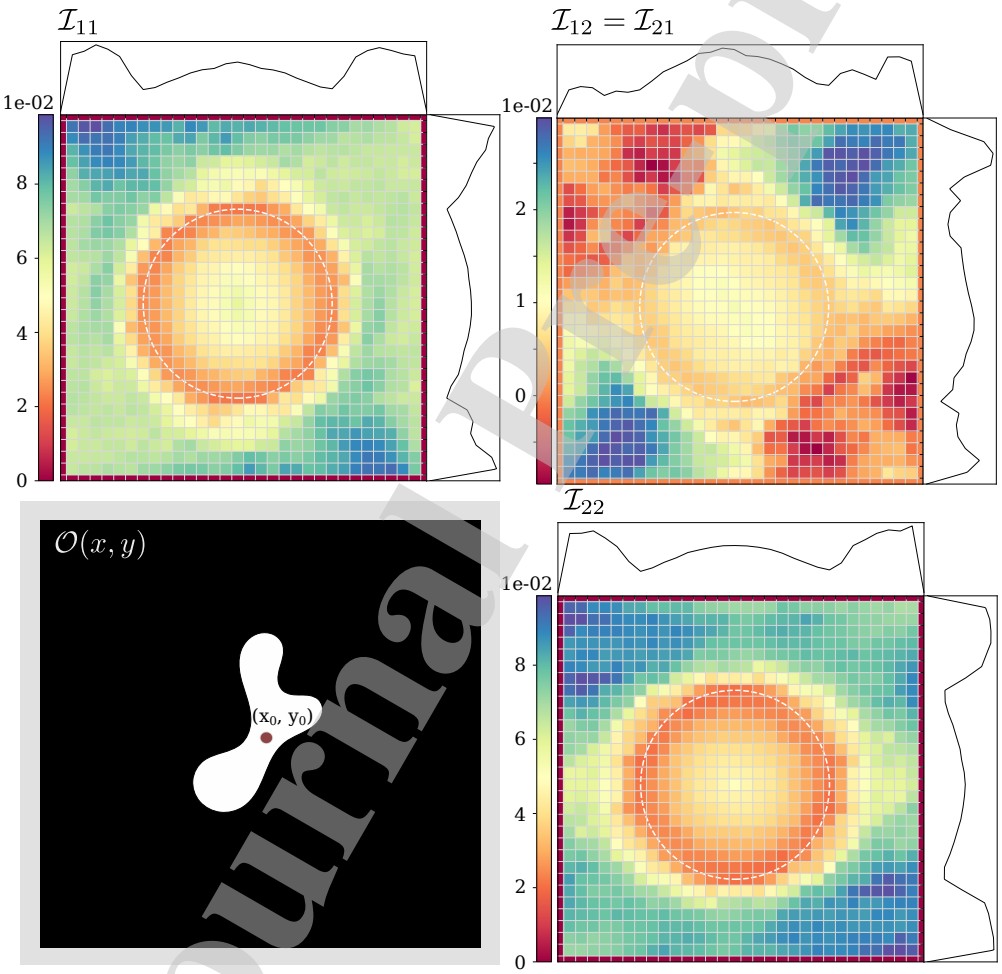

Figure 8: Application of FIM to the estimation of the position of an arbitrary shape. The object $\mathcal{O}$ shown in the bottom left is now the input to the FIM method. The matrices show the information on the x and y positions and its maximum values are dependent on the NA of the system and the shape of the object.

Acknowledgment

The authors would like to thank CONICET for the doctoral fellowship of Juan M. Bujjamer and for providing financial aid for the project. The authors also acknowledge financial support from ANPCYT PICT 2014-3658,Universidad de Buenos Aires 20020130200271BA and MPG Partner Group.

References

[1] G. Zheng, R. Horstmeyer, and C. Yang, "Wide-field, high-resolution Fourier ptychographic microscopy," *Nature Photonics*, vol. 7, pp. 739–745, sep 2013.

[2] M. G. L. Gustafsson, D. a. Agard, and J. W. Sedat, "Doubling the lateral resolution of wide-field fluorescence microscopy using structured illumination," vol. 3919, p. 8007, 2000.

[3] J. R. Fienup, "Phase retrieval algorithms: a personal tour [Invited]," *Applied Optics*, vol. 52, no. 1, p. 45, 2013.

[4] R. A. Gonsalves, "Phase Retrieval And Diversity In Adaptive Optics," *Optical Engineering*, vol. 21, no. 5, pp. 19–22, 1982.

[5] A. Madabhushi and G. Lee, "Image analysis and machine learning in digital pathology: Challenges and opportunities," *Medical Image Analysis*, vol. 33, pp. 170–175, oct 2016.

[6] B. H. Dean and C. W. Bowers, "Diversity selection for phase-diverse phase retrieval," *Journal of the Optical Society of America A*, vol. 20, no. 8, p. 1490, 2003.

[7] M. H. Seaberg, A. D'Aspremont, and J. J. Turner, "Coherent diffractive imaging using randomly coded masks," *Applied Physics Letters*, vol. 107, dec 2015.

[8] A. M. Maiden, M. J. Humphry, M. C. Sarahan, B. Kraus, and J. M. Rodenburg, "An annealing algorithm to correct positioning errors in ptychography," *Ultramicroscopy*, vol. 120, pp. 64–72, 2012.

[9] A. Pan, Y. Zhang, M. Li, M. Zhou, J. Min, M. Lei, and B. Yao, "SNR-based adaptive acquisition method for fast Fourier ptychographic microscopy," *Biomed. Opt. Express*, vol. 7, no. 5, pp. 11394–11403, 2017.

[10] O. Bunk, M. Dierolf, S. Kynde, I. Johnson, O. Marti, and F. Pfeiffer, "Influence of the overlap parameter on the convergence of the ptychographical iterative engine," *Ultramicroscopy*, vol. 108, no. 5, pp. 481–487, 2008.

[11] J. Chao, E. Sally Ward, and R. J. Ober, "Fisher information theory for parameter estimation in single molecule microscopy: tutorial," *Journal of the Optical Society of America A*, vol. 33, no. 7, p. B36, 2016.

[12] D. Bouchet, V. Krachmalnicoff, and I. Izeddin, "Cramér-Rao analysis of lifetime estimations in time-resolved fluorescence microscopy," *Optics Express*, vol. 27, p. 21239, jul 2019.

[13] S. Zhou and L. Jiang, "Modern description of Rayleigh's criterion," *Physical Review A*, vol. 99, p. 013808, jan 2019.

[14] R. Eckert, Z. F. Phillips, and L. Waller, "Efficient illumination angle self-calibration in Fourier ptychography," *Applied Optics*, vol. 57, pp. 1–8, jul 2018.

[15] J. Sun, Q. Chen, Y. Zhang, and C. Zuo, "Sampling criteria for Fourier ptychographic microscopy in object space and frequency space," *Optics Express*, vol. 24, p. 15765, jul 2016.

[16] A. Pan, Y. Zhang, M. Li, M. Zhou, J. Min, M. Lei, and B. Yao, "SNR-based adaptive acquisition method for fast Fourier ptychographic microscopy," *arXiv preprint arXiv:1709.07747*, sep 2017.

[17] L. Bian, J. Suo, G. Situ, G. Zheng, F. Chen, and Q. Dai, "Content adaptive illumination for Fourier ptychography," *Optics Letters*, vol. 39, no. 23, p. 6648, 2014.

[18] K. Guo, S. Dong, P. Nanda, and G. Zheng, "Optimization of sampling pattern and the design of Fourier ptychographic illuminator," *Optics Express*, vol. 23, no. 5, pp. 6171–6180, 2014.

[19] S. Dong, R. Horstmeyer, R. Shiradkar, K. Guo, X. Ou, Z. Bian, H. Xin, and G. Zheng, "Aperture-scanning Fourier ptychography for 3D refocusing and super-resolution macroscopic imaging.," *Optics express*, vol. 22, no. 11, pp. 13586–99, 2014.

[20] Y. Shechtman, Y. C. Eldar, O. Cohen, H. N. Chapman, J. Miao, and M. Segev, "Phase Retrieval with Application to Optical Imaging: A contemporary overview," *IEEE Signal Processing Magazine*, vol. 32, pp. 87–109, may 2015.

[21] V. Elser, "Phase retrieval by iterated projections," *Journal of the Optical Society of America A*, vol. 20, p. 40, jan 2003.

[22] J. R. Fienup, "Reconstruction of an object from the modulus of its Fourier transform," *Optics letters*, vol. 3, pp. 27–29, jul 1978.

[23] R. J. Ober, S. Ram, and E. S. Ward, "Localization Accuracy in Single-Molecule Microscopy," *Biophysical Journal*, vol. 86, pp. 1185–1200, feb 2004.

[24] S. M. Kay, *Estimation Theory*, vol. I of *Fundamentals of Statistical Processing*. Pearson, 1st ed., 1993.

[25] S. Zacks, *Parametric Statistical Inference*. Elsevier, 1981.

[26] S. Ram and E. S. Ward, "A stochastic analysis of performance limits for optical microscopes," *Multidimensional Systems and Signal Processing*, vol. 17, no. 1, pp. 27–57, 2006.

[27] M. Fernández-Suárez and A. Y. Ting, "Fluorescent probes for super-resolution imaging in living cells," *Nature Reviews Molecular Cell Biology*, vol. 9, pp. 929–943, dec 2008.

[28] C. Aguerrebere, J. Delon, Y. Gousseau, P. Musé, C. Aguerrebere, J. Delon, Y. Gousseau, P. Musé, C. Aguerrebere, J. Delon, Y. Gousseau, and P. Mus, "Study of the digital camera acquisition process and statistical modeling of the sensor raw data," *HAL*, sep 2012.

[29] J. Sun, C. Zuo, J. Zhang, Y. Fan, and Q. Chen, "High-speed Fourier ptychographic microscopy based on programmable annular illuminations," *Scientific Reports*, vol. 8, no. 1, pp. 1–12, 2018.

[30] X. Ou, R. Horstmeyer, C. Yang, and G. Zheng, "Quantitative phase imaging via Fourier ptychographic microscopy," *Optics letters*, vol. 38, pp. 4845–8, nov 2013.

[31] H. Lu, J. Chung, X. Ou, and C. Yang, "Quantitative phase imaging and complex field reconstruction by pupil modulation differential phase contrast," *Optics Express*, vol. 24, no. 22, p. 25345, 2016.

[32] C. Zuo, J. Sun, J. Li, A. Asundi, and Q. Chen, "Wide-field high-resolution 3D microscopy with Fourier ptychographic diffraction tomography," *Optics and Lasers in Engineering*, vol. 128, p. 106003, may 2020.

Highlights

- A method to calculate the information contained in a Fourier Ptychography Microscopy Dataset, the first to be reported so far.
- Based on calculating the Fisher Information Matrix for a set of estimated sample parameters.
- Allows estimating a priori the convergence of the reconstruction and therefore enables reducing the acquisition time by selecting only a subset of the data.

LABORATORIO DE ELECTRÓNICA CUÁNTICA
Departamento de Física • Facultad de Ciencias Exactas y Naturales • Universidad de Buenos Aires

On behalf of all authors, I declare no conflict of interests.

Dr. Hernán E. Grecco

Intendente Güiraldes 2160 • Pabellón 1 Ciudad Universitaria • C1428EHA Buenos Aires • Argentina
+54 (11) 4576-3426 • www.lec.df.uba.ar